

Chemical Science

Accepted Manuscript

This article can be cited before page numbers have been issued, to do this please use: D. R. McCarthy, K. Xu, M. Schenkelberg, N. A. Balegamire, H. Liang, S. Bellino, J. Li and S. T. Schneebeli, *Chem. Sci.*, 2024, DOI: 10.1039/D3SC04412B.



This is an Accepted Manuscript, which has been through the Royal Society of Chemistry peer review process and has been accepted for publication.

Accepted Manuscripts are published online shortly after acceptance, before technical editing, formatting and proof reading. Using this free service, authors can make their results available to the community, in citable form, before we publish the edited article. We will replace this Accepted Manuscript with the edited and formatted Advance Article as soon as it is available.

You can find more information about Accepted Manuscripts in the [Information for Authors](#).

Please note that technical editing may introduce minor changes to the text and/or graphics, which may alter content. The journal's standard [Terms & Conditions](#) and the [Ethical guidelines](#) still apply. In no event shall the Royal Society of Chemistry be held responsible for any errors or omissions in this Accepted Manuscript or any consequences arising from the use of any information it contains.

Edge Article

Received 00th January 20xx,
Accepted 00th January 20xx

DOI: 10.1039/x0xx00000x

Kinetically Controlled Synthesis of Rotaxane Geometric Isomers

Dillon R. McCarthy^{a,†}, Ke Xu,^{b,†} Mica E. Schenkelberg^{a,b}, Nils A. N. Balegamire^{a,b}, Huiming Liang^a, Shea A. Bellino^a, Jianing Li^{a,b}, and Severin T. Schneebeli^{*,a,b}

Geometric isomerism in mechanically interlocked systems — which arises when the axle of a mechanically interlocked molecule is oriented, and the macrocyclic component is facially dissymmetric — can provide enhanced functionality for directional transport and polymerization catalysis. We now introduce a kinetically controlled strategy to control geometric isomerism in [2]rotaxanes. Our synthesis provides the major geometric isomer with high selectivity, broadening synthetic access to such interlocked structures. Starting from a readily accessible [2]rotaxane with a symmetrical axle, one of the two stoppers is activated selectively for stopper exchange by the substituents on the ring component. High selectivities are achieved in these reactions, based on coupling the selective formation reactions leading to the major products with inversely selective depletion reactions for the minor products. Specifically, in our reaction system, the desired (major) product forms faster in the first step, while the undesired (minor) product subsequently reacts away faster in the second step. Quantitative ¹H NMR data, fit to a detailed kinetic model, demonstrates that this effect (which is conceptually closely related to minor enantiomer recycling and related processes) can significantly improve the intrinsic selectivity of the reactions. Our results serve as proof of principle for how multiple selective reaction steps can work together to enhance the stereoselectivity of synthetic processes forming complex mechanically interlocked molecules.

Complex interlocked molecules have become integral components for the development of next-generation supramolecular catalysts¹, molecular machines², and molecular motors³. In particular, rotaxanes with either oriented tracks⁴ or facially dissymmetric macrocycles⁵ have shown promise for ribosome-inspired peptide synthesis⁶ and cargo transport.⁷ To impart additional degrees of spatial control and unidirectionality into these systems, it would be desirable to combine oriented axles with facially dissymmetric (i.e. rim-differentiated) macrocyclic components in a selective fashion, which leads to geometric isomers.⁸

We now report a through-space controlled⁹ aminolysis reaction, which can selectively form specific geometric isomers of [2]rotaxanes under kinetic control. Our approach starts with a readily accessible [2]rotaxane with a symmetric axle, which is then desymmetrized based on selective stopper exchange accelerated¹⁰ by the presence of nearby glyme functional groups. We have recently applied this concept in the context of interlocked molecules with through-space glyme-activating groups (Figure 1a), which enabled the two reactive ends in rotaxanes to communicate with each other.¹⁰ However, in our initial system, the ring components of the rotaxanes were facially symmetrical. Therefore, our initial system did not address the complexity of forming specific rotaxane geometric isomers selectively, which has now been accomplished in this

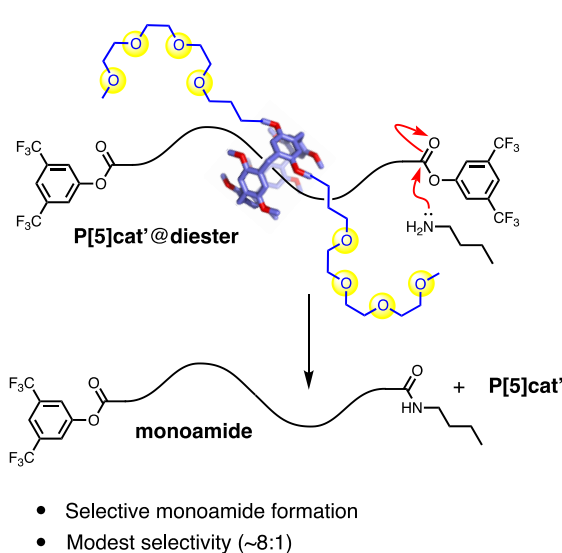
work. Furthermore, in our initial glyme-catalyzed rotaxane system (Figure 1a), we had observed only modest selectivity for the glyme-activated reactions with the maximum selectivity for mono- vs. difunctionalization ~8:1 at the beginning of the reaction.¹⁰ Overall, our glyme-activated directional stopper-exchange process represents an alternative way to accomplish kinetic selection of reaction barriers in interlocked molecules. Our results complement existing approaches to control/augment chemical reactivity through space across the mechanical bond.¹¹ Related processes have also been implemented in chemically fueled molecular machines, where the position^{2a, 12} or facial dissymmetry¹³ of the macrocycle determine the rate of addition and/or removal or a barrier.

Here, we now find that the selectivity for forming specific rotaxane geometric isomers increases exponentially during such glyme-activated reactions. After ~300 hours, the *d.r.* for formation of the major geometric isomer increases to >40:1, which represents a remarkable improvement from the prior 8:1 ratio. Our reactions lead (Figure 1B) to specific rotaxane geometric isomers with high selectivity. This improved selectivity was enabled by coupling (Scheme 1) two through-space controlled aminolysis reactions^{8f, 10, 14} with each other: The first reaction leads to the major geometric isomer with modest selectivity, while the second through-space controlled aminolysis reaction selectively depletes the minor product. Thereby, the overall selectivity of the coupled reaction system is enhanced significantly compared to the two individual reactions. While this concept is related to minor enantiomer recycling¹⁵ and related photo-deracemization processes¹⁶, the minor isomer is not recycled in our system. Therefore, while the selectivity rapidly increases over time (which can lead to simpler purification), the increased selectivity arises at the cost of the overall yield in our system, which decreases over time.

^a Departments of Chemistry, Pathology, and Materials Science Program, University of Vermont, Burlington, VT 05405 (USA).^b Departments of Industrial & Molecular Pharmaceutics, Chemistry, and Medicinal Chemistry & Molecular Pharmacology, Purdue University, West Lafayette, IN 47907 (USA)* Email: Schneebeli@purdue.edu; [†]Equal authorship contribution.

Electronic Supplementary Information (ESI) available: [details of any supplementary information available should be included here]. See DOI: 10.1039/x0xx00000x

a) Ref. 10 (Through-space controlled aminolysis)



b) This work (geometric-isomer selective aminolysis)

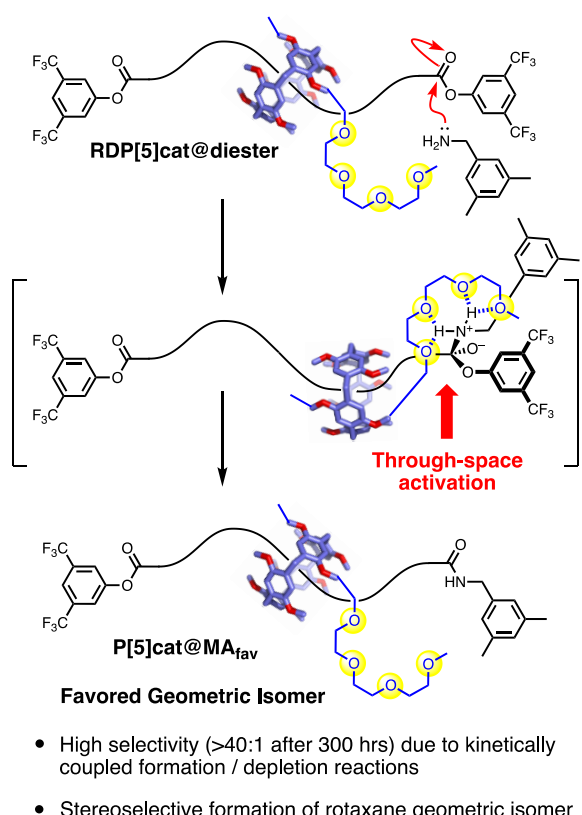
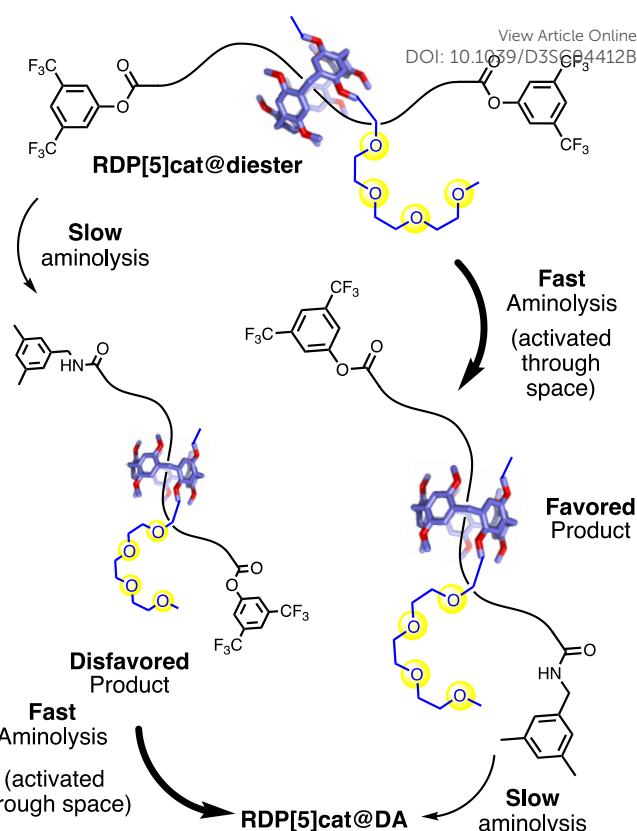


Figure 1. Through-space controlled aminolysis in rotaxane systems. This work applies the concept to the selective synthesis of rotaxane geometric isomers, while also introducing a strategy to enhance the selectivity in such reactions by coupling (see also Scheme 1) a formation reaction selective for the major geometric isomer with a depletion reaction with inverse selectivity.



Scheme 1. A matrix of fast and slow aminolysis reactions (all fast ones are through-space controlled by the glyme-activating groups) leads to kinetic control of geometric isomerism with >40:1 selectivity for the major geometric isomer.

To establish proof-of-concept for our kinetically controlled synthesis, a rim-differentiated pillar[5]arene¹⁷ was chosen as the facially dissymmetric macrocycle given the ease of synthesis¹⁸, excellent chemical stability and solubility¹⁹, and the ability to control the directionality of the catalyst/activating group^{17, 20}. The triglyme activating group (needed to selectively enhance the rate of stopper exchange as illustrated in Figure 1B) is readily installed and is a known^{10, 14a-d, 21} organocatalyst for aminolysis reactions in relatively nonpolar organic solvents like chloroform. With these building blocks in hand, we synthesized **RDP[5]cat@diester** (Scheme 1) in 54% yield by threading^{10, 22} the rim-differentiated pillar[5]arene **RDP[5]cat** (synthesis detailed in the supplementary information) onto a hexadecanedioic acid dichloride axle in the presence of excess 3,5-bis(trifluoromethyl)phenol stopper and triethylamine. Next, we subjected **RDP[5]cat@diester** to aminolysis with 3,5-dimethylbenzylamine at 30 °C. We worked up the reaction early (after 60 hours), to ensure that we could isolate both the major and the minor geometric isomers of the mono-amide products as the NMR standards for the quantitative ¹H NMR experiments (Figure 3). As measured by ¹H NMR spectroscopy (see Figure 3c), the minor geometric isomer disappears almost completely at later time points.

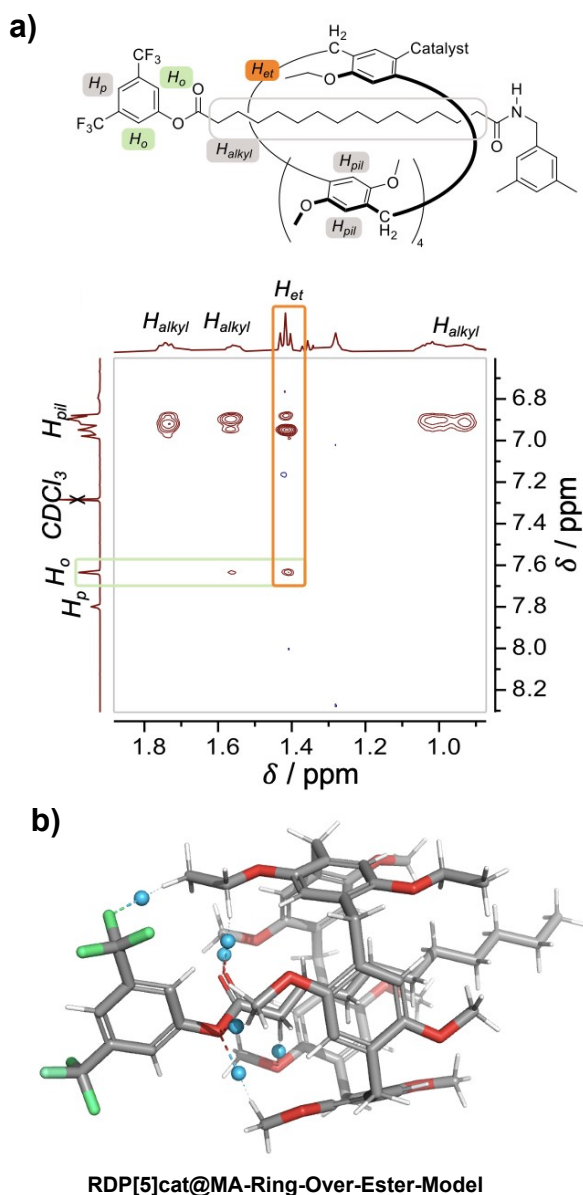


Figure 2. a) Partial ^1H - ^1H ROESY NMR (500 MHz, CDCl_3) spectrum of the major geometric isomer (**RDP[5]cat@MA_{fav}**) obtained from the aminolysis reaction of **RDP[5]cat@diester** with 3,5-dimethylbenzylamine. See the supplementary information for additional characterization data as well as the full ^1H - ^1H ROESY NMR spectrum. The ^1H - ^1H ROESY spectrum shown in the Figure clearly shows that the ethyl group on the pillar[5]arene ring is located proximal to the remaining active ester present in the axle of the favored geometric rotaxane isomer. The key NOE cross-peak between *H_{et}* and *H_o* — which leads us to this conclusion — is highlighted in orange. b) Non-covalent interaction plots²³ calculated at the B3LYP-MM/LACVP* level of theory with the NCI method implemented in Jaguar (version 8.8) as detailed in the supplementary information. The NCI plots show the presence of attractive [C-H]..F interactions between the ethyl groups on the pillararene ring and one of the -CF₃ functionalities of the 3,5-bis(trifluoromethyl)phenyl stopper. We hypothesize that these non-covalent interactions are primarily responsible for biasing the equilibrium distribution of the pillararene ring toward the side of the active-ester stopper, which results in the clear NOE cross-peak shown in panel a.

The glyme-activated stopper-exchange reaction with a first amine nucleophile (3,5-dimethylbenzylamine) led to a mixture of three aminolysis products, which included the two geometric isomers of the mono-substituted rotaxanes **RDP[5]cat@MA_{fav}** and **RDP[5]cat@MA_{disfav}**, as well as the disubstituted rotaxane **RDP[5]cat@DA** in 96% combined yield (calculated based on recovered starting material). The excess amine in the reaction mixture posed a challenge during the workup as attempts to remove the solvent increased the amine concentration, which led to the complete substitution of the remaining active esters. Therefore, we developed a protocol (see supplementary information for details) to remove the excess 3,5-dimethylbenzylamine reagent by simple filtration through an acid-chloride functionalized MP carboxylic acid resin before concentration and purification of the reaction mixture.

The structures of the reaction products with the 3,5-dimethylbenzylamine nucleophile (**RDP[5]cat@MA_{fav}**, **RDP[5]cat@MA_{disfav}**, **RDP[5]cat@DA**) were confirmed with ^1H NMR, ^{13}C NMR, and ^1H - ^1H ROESY NMR spectroscopy, as well as with high-resolution mass spectrometry (see the supplementary information). Notably, the ^1H - ^1H ROESY NMR spectrum of the major, monosubstituted rotaxane product **RDP[5]cat@MA_{fav}** (Figure 2a) shows a cross peak between the *H_{et}* proton resonance (the -CH₃ proton resonance of the ethyl group on the pillar[5]arene macrocycle, observed as a triplet at 1.41 ppm) and the *H_o* aromatic resonance at 7.64 ppm (which corresponds to the *ortho*-protons on the remaining active-ester stoppering unit). The presence of this cross-peak seems to indicate that the pillar[5]arene macrocycle possesses an energetically favorable co-conformation, in which the ring binds to the remaining active ester stopper.

To investigate the origin of this attractive interaction between the ring and the active ester stopper, we optimized a DFT model (Figure 2b) of the corresponding complex and calculated the noncovalent interactions from the DFT-optimized electron density with the NCI method.²³⁻²⁴ Based on our DFT results, there are attractive [C-H]..O and [C-H]..F interactions (illustrated as blue spheres in Figure 2b), which seem to be playing a key role in stabilizing the co-conformation with the pillar[5]arene macrocycle residing next to the active-ester stopper.

Finally, to confirm our kinetic model for the reaction with the 3,5-dimethylbenzylamine nucleophile, we conducted detailed kinetic studies with quantitative ^1H NMR spectroscopy to investigate the selectivity of the reaction over time. For this purpose, **RDP[5]cat@diester** was reacted with an excess of 3,5-dimethylbenzylamine in CDCl_3 at 30 °C in an NMR tube. Our reaction system is governed by four rate constants, k_1 , k_1' , k_2 , and k_2' as defined in Figure 3a. Reaction progression was monitored by ^1H NMR in CDCl_3 using 1,2,4,5-tetrabromobenzene (TBB) as the internal standard. The unique amide protons for all three rotaxane products were readily apparent (Figure 3b), which allowed us to integrate them against the internal TBB standard to yield absolute concentrations. The resulting concentration-time plots

(Figure 3c) were fit to the kinetic model shown in Figure 3a with Dynafit²⁵, providing the four rate constants k_1 , k_2 , k'_1 , and k'_2 . The kinetic model showed that the rate constant corresponding to the formation of the favored rotaxane **RDP[5]cat@MA_{fav}-1** ($k_1 = 0.55 \pm 0.03$) is about an order of magnitude larger than the corresponding rate constant for formation of the disfavored rotaxane **RDP[5]cat@MA_{disfav}-1** ($k_2 = 0.08 \pm 0.005$). Moreover, both k_1 and k'_1 are also about an order of magnitude larger than either k_2 or k'_2 , demonstrating the increased reactivity at the end of the rotaxane nearest to the catalyst.

Our Dynafit model, which was fit to the quantitative ^1H NMR data shown in Figure 3c, provides concentrations of 0.70 mM for **RDP[5]cat@MA_{fav}-1** and 0.02 mM for **RDP[5]cat@MA_{disfav}-1**

at ~ 250 hours, which leads to a selectivity of approximately 31:1 View Article Online
DOI: 10.1039/C4SC00323A
© The Royal Society of Chemistry 2014
Published on 01 February 2014. Downloaded on 2/8/2024 7:45:46 PM.
This article is licensed under a Creative Commons Attribution-NonCommercial 3.0 Unported Licence. $d.r.$ at this reaction time point. After 300 hours, the selectivity for the formation of the major geometric isomer rises even further to about $\sim 45:1$. This finding provides proof of principle for the enhanced selectivity enabled by our kinetically coupled reaction system.

With the kinetic model established for 3,5-dimethylbenzylamine as the nucleophile, we generalized (Figure 4) our selective rotaxane synthesis to other amine nucleophiles, including 1-naphthalenemethanamine and 9-anthracenemethanamine.

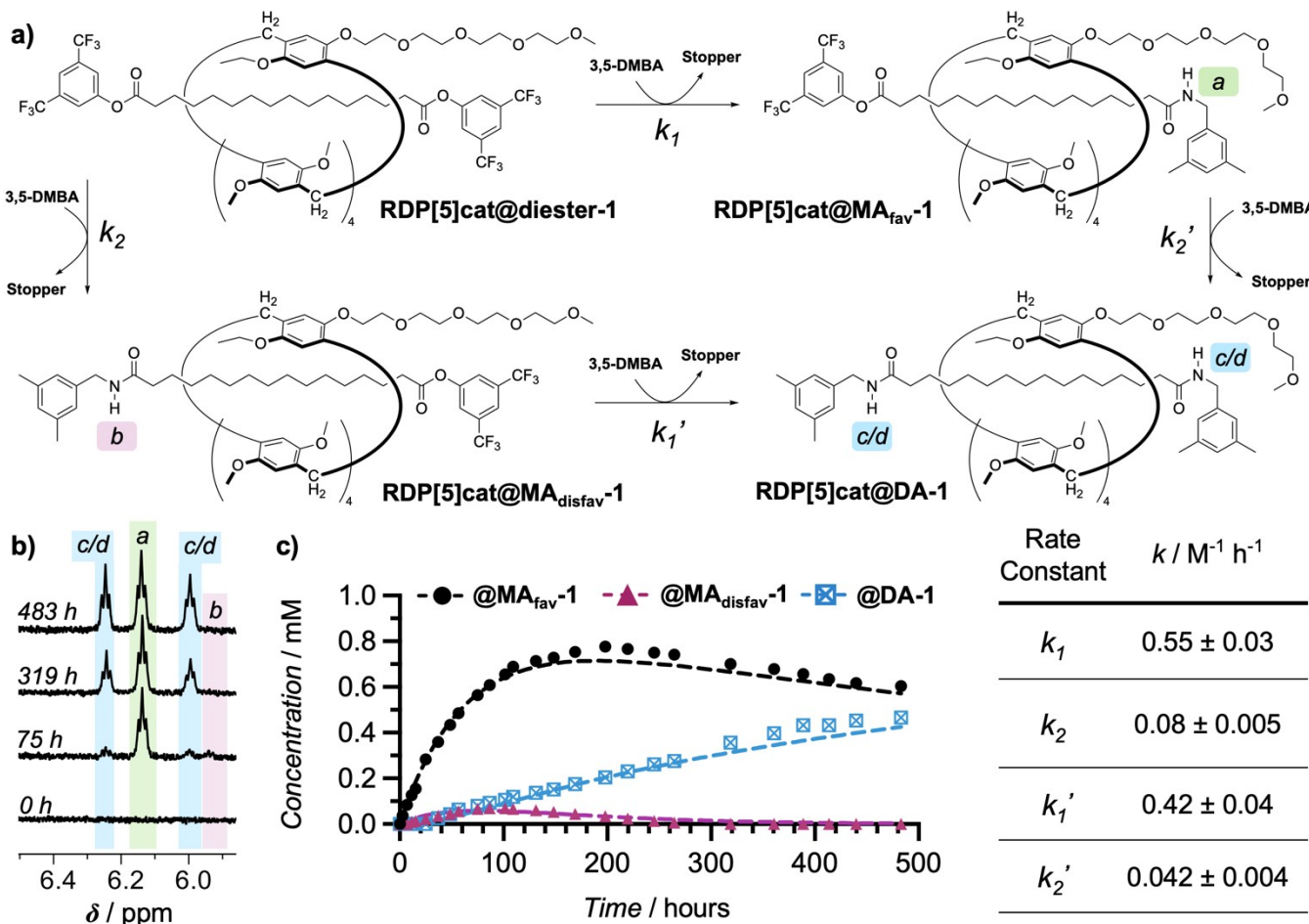
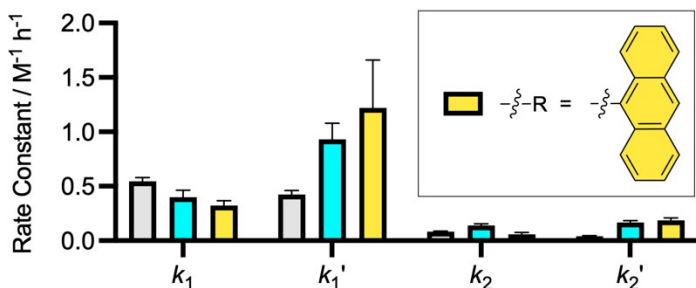


Figure 3. a) Complete kinetic pathway for through-space controlled stopper exchange with 3,5-dimethylbenzylamine as the nucleophile. 3,5-DMBA = 3,5-dimethylbenzylamine; Stopper = 3,5-bis(trifluoromethyl)phenol. Rate constants k_1 and k'_1 denote substitution at the activated ester (proximal to the catalyst the side-chain), while k_2 and k'_2 denote substitution at the ester distal to the catalyst. b) Four representative ^1H NMR spectra (500 MHz, CDCl_3 , 300 K) recorded at different time points over the course of the kinetics experiment. The three sets of amide protons (1 NH each for both **RDP[5]cat@MA_{fav}** and **RDP[5]cat@MA_{disfav}**, 2 NH for **RDP[5]cat@DA**) are highlighted. A complete stack of the entire kinetics spectrum is shown in Figure S1 in the supplementary information. c) Concentrations of all three reaction products measured by quantitative ^1H NMR spectroscopy with the TBB internal standard over the course of the reaction. The reaction was run at 30 °C as detailed in the supplementary information. Kinetics fits are shown as dashed lines. The kinetic fits were obtained using the Dynafit software package as detailed in the supplementary information. Derived rate constants with error bars (standard errors obtained from the Dynafit kinetic fits) are shown in the table on the right.



[View Article Online](#)
DOI: 10.1039/DTCS04412B

Trends explained by sterics and varying ring-with-amide interaction strengths (Fig. 6)

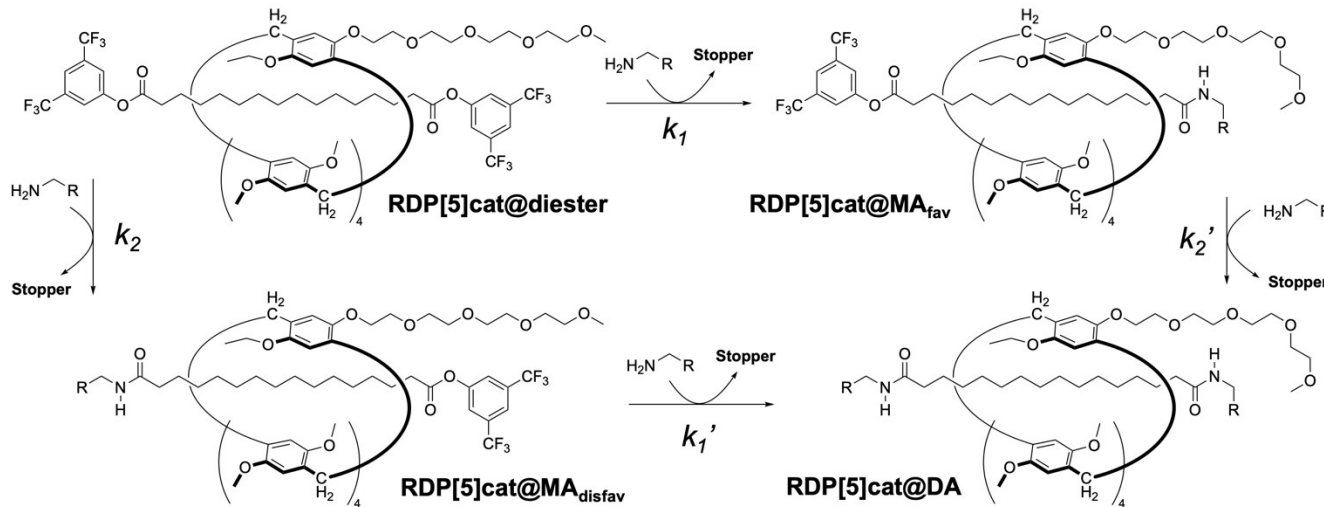
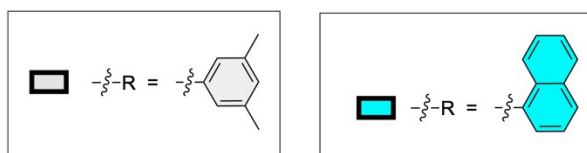


Figure 4. Comparison of aminolysis rate constants for **RDP[5]cat@diester** with different amine nucleophiles. All reactions were run at 30 °C as detailed in the supplementary information. See Figures S1–S5 for the kinetic fits and stacks of the time-dependent ^1H NMR spectra, which were used to determine all the rate constants. The kinetic fits were obtained using the Dynafit software package as detailed in the supplementary information. Numerical values for the derived rate constants with error bars (standard errors obtained from the Dynafit kinetic fits) are listed in Figures 3c, S3b, and S5b.

Both systems performed qualitatively similar to the reaction system with the 3,5-dimethylbenzylamine, which confirms the generality of our kinetically controlled rotaxane geometric isomer synthesis. However, we also observed (Figures 4 and 6) clear trends in the rate constants, based on (i) the sterics of the nucleophiles/amide stoppers and (ii) the sterics of the secondary (non-activating) face of the ring, which (when positioned over an active ester) seems to slow down the aminolysis reactions.

(i) Steric effects of the nucleophile/amide stopper on the aminolysis rates: First, the observed trend in k_1 rate constants (Figure 4) clearly shows that the k_1 rate constants decrease with increasing steric bulk of the nucleophile, as one would expect for a classical acyl substitution mechanism.

At the same time, the rate constants k_1' increased significantly from $R = 3,5$ -dimethylbenzyl, to $R = 1$ -naphthyl, and $R = 9$ -anthracenyl, which is contrary to the trend observed for k_1 . We hypothesize that this inverted trend is the result of reduced supramolecular interactions between the pillararene ring and the amide stoppers in the monofunctionalized rotaxane products **RDP[5]cat@MA_{disfav}-2** (the napthyl case) and

RDP[5]cat@MA_{disfav}-3 (the anthracenyl case). This hypothesis was confirmed by DFT-calculated binding energies (Figure 6) between the ring and the amide stoppers.

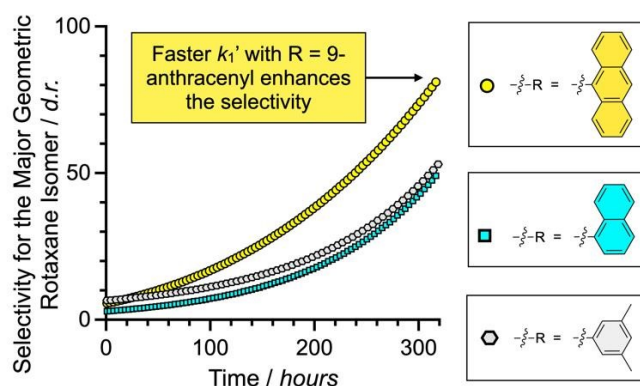


Figure 5. Plots of the diastereoselectivity ($d.r. = [\text{RDP[5]cat@MA}_{\text{fav}}] / [\text{RDP[5]cat@MA}_{\text{disfav}}]$) for the major geometric rotaxane isomers formed over time for the aminolysis reactions shown in Figure 4. The concentrations of the products were obtained from the kinetic fits to the quantitative ^1H NMR data shown in Figures 3, S3b, and S5b.

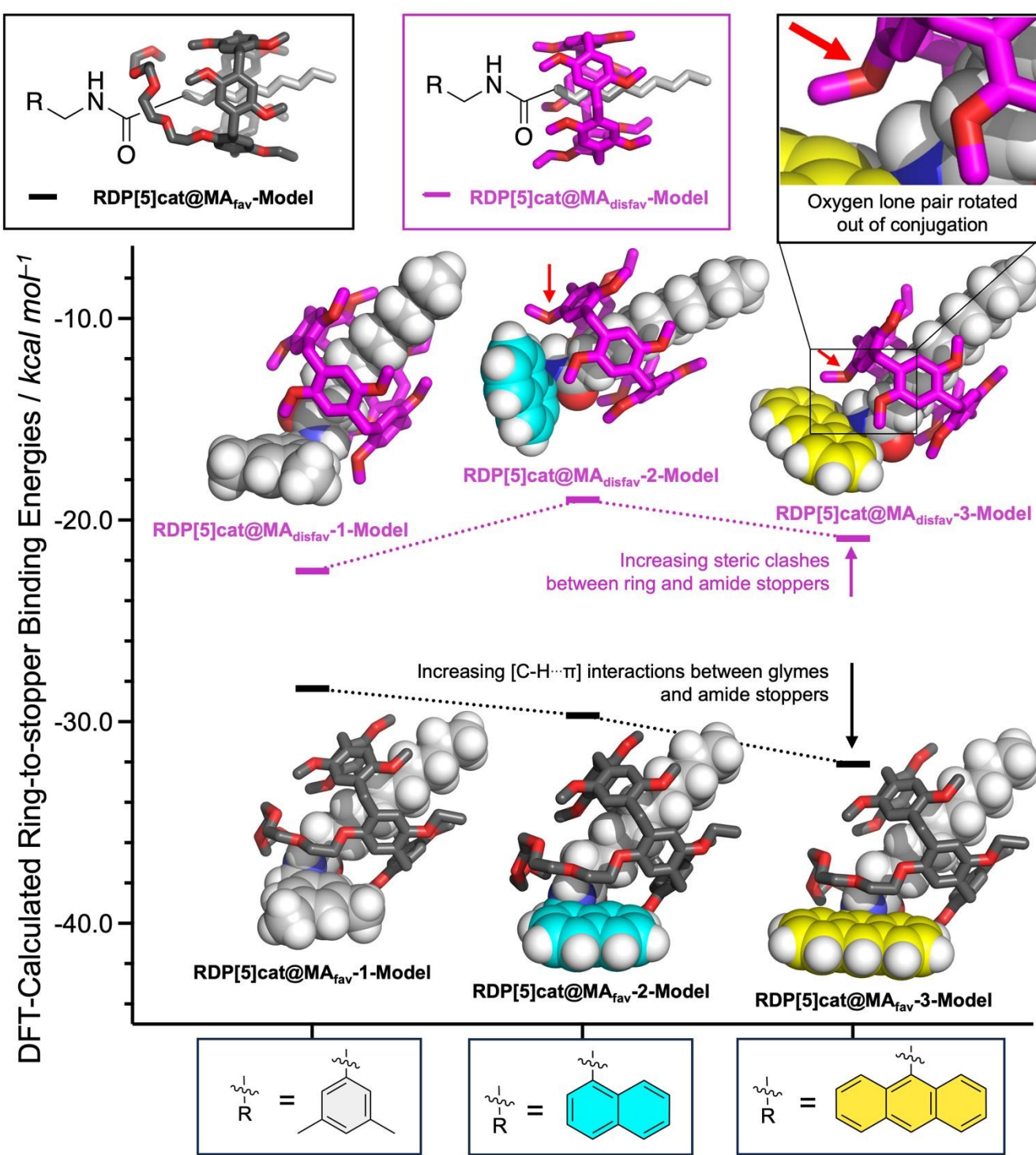


Figure 6. DFT-calculated binding energies (B3LYP-MM/aug-cc-pVDZ//B3LYP-MM/LACVP* level of theory) between the different faces of the **RDP[5]cat** ring and the varying amide stoppers for both geometric isomers. The model systems used to calculate the binding energies are shown in insets at the top left of the figure. In the model systems for the disfavored rotaxane products (**RDP[5]cat@MA_{disfav}-1-Model**, **RDP[5]cat@MA_{disfav}-2-Model**, and **RDP[5]cat@MA_{disfav}-3-Model**), the tetraglyme chains do not directly interact with the varying amide stoppers. Therefore, for the models of the disfavored rotaxane products, the tetraglyme chains on the ring were replaced with ethyl substituents to simplify the conformational space and enable a more accurate search of the conformational space at the DFT level with these smaller model systems.

Based on the DFT results, we find that 3,5-dimethylbenzylamide stopper in **RDP[5]cat@MA_{disfav}-1** binds the strongest with the pillararene ring, while the 9-anthracenemethanamide and the 1-naphthalenemethanamide stoppers showed a reduced affinity with the ring.

Once again, this trend is caused by the increasing steric bulk of the initial amine nucleophiles, which ultimately leads to bulkier amide stoppers in the anthracenyl/naphthyl cases for the monofunctionalized rotaxane products **RDP[5]cat@MA_{disfav}**. As shown by our DFT calculations (Figure 6), the increased steric bulk of the 9-anthracenemethanamide and the 1-naphthalenemethanamide stoppers even forces one of the methoxyl groups out of conjugation with the aromatic units on the pillararene rings. As a result, the supramolecular interaction strength between the rings and the amide stoppers is significantly reduced in the anthracenyl/naphthyl cases, which favors the co-conformations with the glyme activating groups residing over the remaining active esters. Consequently, the k_1' rate constants with **RDP[5]cat@MA_{disfav}-2** and **RDP[5]cat@MA_{disfav}-3** are faster than with **RDP[5]cat@MA_{disfav}-1**.

Since the fastest k_1' results with 9-anthracenemethanamine as the nucleophile, the minor geometric rotaxane isomer (**RDP[5]cat@MA_{disfav}**) reacts away even faster in the anthracenyl case, which further increases the selectivity for the formation of the major geometric isomer (as shown in Figure 5) with 9-anthracenemethanamine as the nucleophile. Overall, near exponential growth of the reaction selectivity over time is observed (Figure 5) with all three amine nucleophiles, since — as more of the desired major product forms over time — the undesired product also keeps reacting away faster than the desired product, which leads to a continuously increasing selectivity of the reaction for the major geometric isomer.

(ii) Steric effects of the ring on the aminolysis rates: While the face of the ring with the tetraglyme chains clearly speeds up the aminolysis reactions as discussed above, the aminolysis reactions slow down when the secondary face of the ring (i.e., the face without the glyme functions) is sitting over an active ester. Based on our computational model shown in Figure 2b, we explain this slow-down effect by the simple steric bulk of the macrocycle, which partially blocks attack of the nucleophile when the secondary face of the ring is positioned over the active ester. Related inhibition effects of reactivity by the mechanical bond have been observed previously in the literature.²⁶

This inhibition effect is also clearly visible when comparing the k_2 and k_2' rate constants (Figure 3c) for the aminolysis reaction with 3,5-dimethylbenzylamine. In this case, k_2' is significantly slower than k_2 , since in the monoamide **RDP[5]cat@MA_{fav}-1** the ring spends a significant portion of time over the active ester (based on the NOESY NMR shown in Figure 2a), thereby partially blocking access of the nucleophile to the active ester in this

monoamide. In contrast, the ring is expected to be much more evenly distributed between the two active ester sites in the starting material **RDP[5]cat@diester**, which ultimately leads to k_2 being significantly faster than k_2' with the 3,5-dimethylbenzylamine nucleophile.

At the same time, the k_2' rate constants also increased notably (Figure 4) in the anthracenyl and naphthyl cases, compared to the case with R = 3,5-dimethylbenzyl. Again, we hypothesize that this effect is caused by the secondary face of the ring inhibiting nucleophilic attack, and by changing the balance of supramolecular interactions between the ring and the varying amide stoppers. In this case, the DFT calculations show that the tetraglyme groups interact²⁷ more strongly with the amide stoppers when R = naphthyl/anthracenyl than with R = 3,5-dimethylbenzyl. Therefore, the stronger supramolecular interactions between the tetraglyme groups and the aromatic stoppers in the anthracenyl/naphthyl case favor the conformation with the ring residing over the side of the amide stopper in the case of **RDP[5]cat@MA_{fav}-2** and **RDP[5]cat@MA_{fav}-3**, which frees up the active ester on the other end of the rotaxane for faster nucleophilic attack and leads to overall faster k_2' rate constants.

Conclusions

We developed a kinetically controlled strategy to selectively access specific geometric isomers of complex interlocked molecules through a coupled reaction system involving selective stopper exchange reactions. Our reaction system was able to achieve high selectivity by enhancing the intrinsic selectivity of the selective stopper exchange reactions based on coupled reactions of inverse selectivity. While the use of a glyme catalyst/activating group as a means of promoting stopper exchange in rotaxanes was previously reported by our group¹⁰, this work expands the synthetic toolbox available to selectively access rotaxane geometric isomers. We are currently applying our synthetic strategy for the synthesis of new living polymerization catalysts and are also expanding our methodology to other macrocycles and catalysts/activating groups to access complex interlocked molecules in a more effective manner.

Author Contributions

S.T.S. guided the project, performed the DFT calculations together with D.R.M. and K.X., discussed the experimental results, and wrote the paper together with D.R.M. and K.X. D.R.M., K.X., N.B., H.L., and S.B. performed the synthesis and analysed the data. All the authors discussed the results and revised the paper.

Conflicts of interest

There are no conflicts to declare.

Acknowledgements

We thank M. Ivancic for NMR support and B. O'Rourke for high-resolution mass spectrometry. Synthetic material for this research was supported by the NSF (CAREER Award CHE-1848444/2317652 awarded to STS), while the kinetic analysis was supported by the U.S. Army Research Office (Grant 71015-CH-YIP awarded to STS). Part of the computational resources were supported by the NVIDIA GPU Grant Seed Program (awarded to STS) and by the NIH (MIRA award 1R35GM147579-01). Partial support was also provided by NSF's CTMC Program via an NSF CAREER Award (CHE-1945394) awarded to JL. H.L was supported by a summer undergraduate research fellowship from Middlebury College.

Notes and references

1. a) V. Blanco, A. Carbone, K. D. Hänni, D. A. Leigh and B. Lewandowski, A Rotaxane-Based Switchable Organocatalyst, *Angew. Chem. Int. Ed.*, 2012, **51**, 5166-5169; b) V. Blanco, D. A. Leigh, V. Marcos, J. A. Morales-Serna and A. L. Nussbaumer, A Switchable [2]Rotaxane Asymmetric Organocatalyst That Utilizes an Acyclic Chiral Secondary Amine, *J. Am. Chem. Soc.*, 2014, **136**, 4905-4908; c) Y. Cakmak, S. Erbas-Cakmak and D. A. Leigh, Asymmetric Catalysis with a Mechanically Point-Chiral Rotaxane, *J. Am. Chem. Soc.*, 2016, **138**, 1749-1751; d) K. Eichstaedt, J. Jaramillo-Garcia, D. A. Leigh, V. Marcos, S. Pisano and T. A. Singleton, Switching between Anion-Binding Catalysis and Aminocatalysis with a Rotaxane Dual-Function Catalyst, *J. Am. Chem. Soc.*, 2017, **139**, 9376-9381; e) A. W. Heard and S. M. Goldup, Synthesis of a Mechanically Planar Chiral Rotaxane Ligand for Enantioselective Catalysis, *Chem.*, 2020, **6**, 994-1006; f) C. Kwamen and J. Niemeyer, Functional Rotaxanes in Catalysis, *Chem. Eur. J.*, 2021, **27**, 175-186; g) J. Y. C. Lim, N. Yuntawattana, P. D. Beer and C. K. Williams, Isolelective Lactide Ring Opening Polymerisation using [2]Rotaxane Catalysts, *Angew. Chem. Int. Ed.*, 2019, **58**, 6007-6011; h) A. Martinez-Cueva, A. Saura-Sanmartin, M. Alajarín and J. Berna, Mechanically Interlocked Catalysts for Asymmetric Synthesis, *ACS Catal.*, 2020, **10**, 7719-7733; i) A. Martinez-Cueva, A. Saura-Sanmartin, T. Nicolas-Garcia, C. Navarro, R.-A. Orenes, M. Alajarín and J. Berna, Photoswitchable interlocked thiadiglycolamide as a cocatalyst of a chalcogeno-Baylis-Hillman reaction, *Chem. Sci.*, 2017, **8**, 3775-3780.
2. a) S. Borsley, D. A. Leigh and B. M. W. Roberts, A Doubly Kinetically-Gated Information Ratchet Autonomously Driven by Carbodiimide Hydration, *J. Am. Chem. Soc.*, 2021, **143**, 4414-4420; b) S. F. M. v. Dongen, S. Cantequin, J. A. A. W. Elemans, A. E. Rowan and R. J. M. Nolte, Functional interlocked systems, *Chem. Soc. Rev.*, 2013, **43**, 99-122; c) S. Erbas-Cakmak, D. A. Leigh, C. T. McTernan and A. L. Nussbaumer, Artificial Molecular Machines, *Chem. Rev.*, 2015, **115**, 10081-10206; d) J. Groppi, L. Casimiro, M. Canton, S. Corra, M. Jafari-Nasab, G. Tabacchi, L. Cavallo, M. Baroncini, S. Silvi, E. Fois and A. Credi, Precision Molecular Threading/Dethreading, *Angew. Chem. Int. Ed.*, 2020, **132**, 14935-14944; e) E. R. Kay and D. A. Leigh, Rise of the Molecular Machines, *Angew. Chem. Int. Ed.*, 2015, **54**, 10080-10088; f) J. E. M. Lewis, M. Galli and S. M. Goldup, Properties and emerging applications of mechanically interlocked ligands, *Chem. Commun.*, 2016, **53**, 298-312; g) S. Mena-Hernando and E. M. Pérez, Mechanically interlocked materials. Rotaxanes and catenanes beyond the small molecule, *Chem. Soc. Rev.*, 2019, **48**, 5016-5032; h) E. A. Neal and S. M. Goldup, Chemical consequences of mechanical bonding in catenanes and rotaxanes: isomerism, modification, catalysis and molecular machines for synthesis, *Chem. Commun.*, 2014, **50**, 5128-5142; i) D. Sluysmans, P. Lussis, C.-A. Fustin, A. Bertocco, D. A. Leigh and A.-S. Duwez, Real-Time Fluctuations in Single-Molecule Rotaxane Experiments Reveal an Intermediate Weak Binding State during Shuttling, *J. Am. Chem. Soc.*, 2021, **143**, 2348-2352; j) C. A. Stanier, S. J. Alderman, T. D. W. Claridge and H. L. Anderson, Unidirectional Photoinduced Shuttling in a Rotaxane with a Symmetric Stilbene Dumbbell, *Angew. Chem. Int. Ed.*, 2002, **41**, 1769-1772; k) T. Takata, Switchable Polymer Materials Controlled by Rotaxane Macromolecular Switches, *ACS Cent. Sci.*, 2020, **6**, 129-143; l) P. Wu, B. Dharmadhikari, P. Patra and X. Xiong, Rotaxane nanomachines in future molecular electronics, *Nanoscale Adv.*, 2022, **4**, 3418-3461; m) B. Yao, H. Sun, L. Yang, S. Wang and X. Liu, Recent Progress in Light-Driven Molecular Shuttles, *Front. Chem.*, 2022, **9**; n) H.-Y. Zhou, Q.-S. Zong, Y. Han and C.-F. Chen, Recent advances in higher order rotaxane architectures, *Chem. Commun.*, 2020, **56**, 9916-9936.
3. a) M. Baroncini, S. Silvi and A. Credi, Photo- and Redox-Driven Artificial Molecular Motors, *Chem. Rev.*, 2020, **120**, 200-268; b) Y. Feng, M. Ovalle, J. S. W. Seale, C. K. Lee, D. J. Kim, R. D. Astumian and J. F. Stoddart, Molecular Pumps and Motors, *J. Am. Chem. Soc.*, 2021, **143**, 5569-5591.
4. a) R. J. Bordoli and S. M. Goldup, An Efficient Approach to Mechanically Planar Chiral Rotaxanes, *J. Am. Chem. Soc.*, 2014, **136**, 4817-4820; b) C. Casati, P. Franchi, R. Pievo, E. Mezzina and M. Lucarini, Unraveling Unidirectional Threading of α -Cyclodextrin in a [2]Rotaxane through Spin Labeling Approach, *J. Am. Chem. Soc.*, 2012, **134**, 19108-19117; c) F. d'Orchymont and J. P. Holland, Supramolecular Rotaxane-Based Multi-Modal Probes for Cancer Biomarker Imaging**, *Angew. Chem. Int. Ed.*, 2022, **61**, e202204072; d) E. M. G. Jamieson, F. Modicom and S. M. Goldup, Chirality in rotaxanes and catenanes, *Chem. Soc. Rev.*, 2018, **47**, 5266-5311; e) M. A. Jinks, A. de Juan, M. Denis, C. J. Fletcher, M. Galli, E. M. G. Jamieson, F. Modicom, Z. Zhang and S. M. Goldup, Stereoselective Synthesis of Mechanically Planar Chiral Rotaxanes, *Angew. Chem. Int. Ed.*, 2018, **57**, 14806-14810; f) Y. Makita, N. Kihara and T. Takata, Synthesis and kinetic resolution of directional isomers of [2]rotaxanes bearing a lariat crown ether wheel, *Supramol. Chem.*, 2021, **33**, 1-7; g) J. R. J. Maynard and S. M. Goldup, Strategies for the Synthesis of Enantiopure Mechanically Chiral Molecules, *Chem.*, 2020, **6**, 1914-1932; h) K. Nakazono and T. Takata, Mechanical Chirality of Rotaxanes: Synthesis and Function, *Symmetry*, 2020, **12**, 144; i) N. Pairault and J. Niemeyer, Chiral Mechanically Interlocked Molecules – Applications of Rotaxanes, Catenanes and Molecular Knots in Stereoselective Chemosensing and Catalysis, *Synlett*, 2018, **29**, 689-698.
5. a) M. Bazzoni, L. Andreoni, S. Silvi, A. Credi, G. Cera, A. Secchi and A. Arduini, Selective access to constitutionally identical, orientationally isomeric calix[6]arene-based [3]rotaxanes by an



active template approach, *Chem. Sci.*, 2021, **12**, 6419-6428; b) P. La Manna, C. Talotta, C. Gaeta, A. Soriente, M. De Rosa and P. Neri, Threading of an Inherently Directional Calixarene Wheel with Oriented Ammonium Axles, *J. Org. Chem.*, 2017, **82**, 8973-8983.

6. a) G. De Bo, M. A. Y. Gall, M. O. Kitching, S. Kuschel, D. A. Leigh, D. J. Tetlow and J. W. Ward, Sequence-Specific β -Peptide Synthesis by a Rotaxane-Based Molecular Machine, *J. Am. Chem. Soc.*, 2017, **139**, 10875-10879; b) J. Echavarren, M. A. Y. Gall, A. Haertsch, D. A. Leigh, J. T. J. Spence, D. J. Tetlow and C. Tian, Sequence-Selective Decapeptide Synthesis by the Parallel Operation of Two Artificial Molecular Machines, *J. Am. Chem. Soc.*, 2021, **143**, 5158-5165.

7. J. Berná, D. A. Leigh, M. Lubomska, S. M. Mendoza, E. M. Pérez, P. Rudolf, G. Teobaldi and F. Zerbetto, Macroscopic transport by synthetic molecular machines, *Nature Materials*, 2005, **4**, 704-710.

8. a) T. Oshikiri, Y. Takashima, H. Yamaguchi and A. Harada, Kinetic Control of Threading of Cyclodextrins onto Axle Molecules, *J. Am. Chem. Soc.*, 2005, **127**, 12186-12187; b) M. Quiroga, M. Parajó, P. Rodríguez-Dafonte and L. García-Río, Kinetic Study of [2]Pseudorotaxane Formation with an Asymmetrical Thread, *Langmuir*, 2016, **32**, 6367-6375; c) Q.-C. Wang, X. Ma, D.-H. Qu and H. Tian, Unidirectional Threading Synthesis of Isomer-Free [2]Rotaxanes, *Chem. Eur. J.*, 2006, **12**, 1088-1096; d) M. Xue, Y. Yang, X. Chi, X. Yan and F. Huang, Development of Pseudorotaxanes and Rotaxanes: From Synthesis to Stimuli-Responsive Motions to Applications, *Chem. Rev.*, 2015, **115**, 7398-7501; e) T. Oshikiri, Y. Takashima, H. Yamaguchi and A. Harada, Face-Selective [2]- and [3]Rotaxanes: Kinetic Control of the Threading Direction of Cyclodextrins, *Chem. Eur. J.*, 2007, **13**, 7091-7098; f) P. Waelès, M. Gauthier and F. Coutrot, Study of [2]- and [3]Rotaxanes Obtained by Post-Synthetic Aminolysis of a Kinetically Stable Carbonate-Containing Pseudorotaxane, *Europ. J. Org. Chem.*, 2022, **2022**, e202101385; g) H.-X. Wang, Z. Meng, J.-F. Xiang, Y.-X. Xia, Y. Sun, S.-Z. Hu, H. Chen, J. Yao and C.-F. Chen, Guest-dependent directional complexation based on triptycene derived oxacalixarene: formation of oriented rotaxanes, *Chem. Sci.*, 2016, **7**, 469-474.

9. a) M. D. Struble, M. G. Holl, G. Coombs, M. A. Siegler and T. Lectka, Synthesis of a Tight Intramolecular OH \cdots Olefin Interaction, Probed by IR, 1 H NMR, and Quantum Chemistry, *J. Org. Chem.*, 2015, **80**, 4803-4807; b) M. G. Holl, M. D. Struble, P. Singal, M. A. Siegler and T. Lectka, Positioning a Carbon-Fluorine Bond over the π Cloud of an Aromatic Ring: A Different Type of Arene Activation, *Angew. Chem., Int. Ed.*, 2016, **55**, 8266-8269; c) D. D. Bume, C. R. Pitts, F. Ghorbani, S. A. Harry, J. N. Capilato, M. A. Siegler and T. Lectka, Ketones as directing groups in photocatalytic sp 3 C-H fluorination, *Chem. Sci.*, 2017, **8**, 6918-6923; d) L. Guan, M. G. Holl, C. R. Pitts, M. D. Struble, M. A. Siegler and T. Lectka, Through-Space Activation Can Override Substituent Effects in Electrophilic Aromatic Substitution, *J. Am. Chem. Soc.*, 2017, **139**, 14913-14916; e) K. E. Murphy, J. L. Bocanegra, X. Liu, H. K. Chau, P. C. Lee, J. Li and S. T. Schneebeli, Precise through-space control of an abiotic electrophilic aromatic substitution reaction, *Nat. Commun.*, 2017, **8**, 14840; f) C. R. Pitts, M. G. Holl and T. Lectka, Spectroscopic Characterization of a [C-F-C] $+$ Fluoronium Ion in Solution, *Angew. Chem. Int. Ed.*, 2018, **57**, 1924-1927; g) J. P.

Campbell, S. C. Rajappan, T. J. Jaynes, M. Sharifi, Y. T. Ma, J. Li and S. T. Schneebeli, Enantioselective Electrophilic Aromatic Nitration: A Chiral Auxiliary Approach, *Angew. Chem. Int. Ed.*, 2019, **58**, 1035-1040; h) M. Kazim, H. Foy, M. A. Siegler, T. Dudding and T. Lectka, Discovery and Mechanistic Study of a Totally Organic C(aryl)-C(alkyl)Oxygen Insertion Reaction, *J. Org. Chem.*, 2019, **84**, 14349-14353; i) M. Kazim, M. A. Siegler and T. Lectka, A Case of Serendipity: Synthesis, Characterization, and Unique Chemistry of a Stable, Ring-Unsubstituted Aliphatic p-Quinone Methide, *Org. Lett.*, 2019, **21**, 2326-2329; j) M. G. Holl, C. R. Pitts and T. Lectka, Quest for a Symmetric [C-F-C] $+$ Fluoronium Ion in Solution: A Winding Path to Ultimate Success, *Acc. Chem. Res.*, 2020, **53**, 265-275; k) M. Kazim, L. Guan, A. Chopra, R. Sun, M. A. Siegler and T. Lectka, Switching a HO \cdots π Interaction to a Nonconventional OH \cdots π Hydrogen Bond: A Completed Crystallographic Puzzle, *J. Org. Chem.*, 2020, **85**, 9801-9807; l) S. T. Schneebeli, M. Sharifi, J. P. Campbell, K. E. Murphy and R. Osadchey Brown, Chiral Auxiliaries for Stereoselective Electrophilic Aromatic Substitutions, *Synlett*, 2020, **32**, 229-234; m) K. F. Hoffmann, A. Wiesner, C. Mueller, S. Steinhauer, H. Beckers, M. Kazim, C. R. Pitts, T. Lectka and S. Riedel, Structural proof of a [C-F-C] $+$ fluoronium cation, *Nat. Commun.*, 2021, **12**, 5275; n) S. A. Harry, M. R. Xiang, E. Holt, A. Zhu, F. Ghorbani, D. Patel and T. Lectka, Hydroxy-directed fluorination of remote unactivated C(sp 3)-H bonds: a new age of diastereoselective radical fluorination, *Chem. Sci.*, 2022, **13**, 7007-7013; o) M. Kazim, Z. Feng, S. Vemulapalli, M. A. Siegler, A. Chopra, P. Minh Nguyen, M. Gargiulo Holl, L. Guan, T. Dudding, D. J. Tantillo and T. Lectka, Through-Space, Lone-Pair Promoted Aromatic Substitution: A Relay Mechanism Can Beat Out Direct Activation, *Chem. Eur. J.*, 2023, DOI: 10.1002/chem.202301550, e202301550; p) M. Kazim, M. Wang, S. Vemulapalli, P. M. Nguyen, Y. Wang, M. A. Siegler, T. Dudding and T. Lectka, How Do Face-to-Face Stacked Aromatic Rings Activate Each Other to Electrophilic Aromatic Substitution?, *Org. Lett.*, 2023, **25**, 4318-4322; q) H. J. Davis and R. J. Phipps, Harnessing non-covalent interactions to exert control over regioselectivity and site-selectivity in catalytic reactions, *Chem. Sci.*, 2017, **8**, 864-877; r) W. A. Golding, R. Pearce-Higgins and R. J. Phipps, Site-Selective Cross-Coupling of Remote Chlorides Enabled by Electrostatically Directed Palladium Catalysis, *J. Am. Chem. Soc.*, 2018, **140**, 13570-13574; s) W. A. Golding and R. J. Phipps, Electrostatically-directed Pd-catalysis in combination with C-H activation: site-selective coupling of remote chlorides with fluoroarenes and fluoroheteroarenes, *Chem. Sci.*, 2020, **11**, 3022-3027; t) Y.-H. Li, Y. Ouyang, N. Chekshin and J.-Q. Yu, PdII-Catalyzed γ -C(sp 3)-H (Hetero)arylation of Ketones Enabled by Transient Directing Groups, *ACS Catal.*, 2022, **12**, 10581-10586; u) Y.-Q. Chen, S. Singh, Y. Wu, Z. Wang, W. Hao, P. Verma, J. X. Qiao, R. B. Sunoj and J.-Q. Yu, Pd-Catalyzed γ -C(sp 3)-H Fluorination of Free Amines, *J. Am. Chem. Soc.*, 2020, **142**, 9966-9974; v) K. Hong, H. Park and J.-Q. Yu, Methylene C(sp 3)-H Arylation of Aliphatic Ketones Using a Transient Directing Group, *ACS Catal.*, 2017, **7**, 6938-6941; w) Y. Wu, Y.-Q. Chen, T. Liu, M. D. Eastgate and J.-Q. Yu, Pd-Catalyzed γ -C(sp 3)-H Arylation of Free Amines Using a Transient Directing Group, *J. Am. Chem. Soc.*, 2016, **138**, 14554-14557; x) G. Xia, J. Weng, L. Liu, P. Verma, Z. Li and J.-Q. Yu, Reversing conventional site-selectivity in C(sp 3)-H bond activation, *Nat. Chem.*, 2019, **11**, 571-577; y) L.-J. Xiao, K. Hong, F. Luo, L. Hu, W. R. Ewing, K.-S. Yeung and J.-Q. Yu, PdII-

Catalyzed Enantioselective C(sp₃)-H Arylation of Cyclobutyl Ketones Using a Chiral Transient Directing Group, *Angew. Chem., Int. Ed.*, 2020, **59**, 9594-9600; z) F.-L. Zhang, K. Hong, T.-J. Li, H. Park and J.-Q. Yu, Functionalization of C(sp₃)-H bonds using a transient directing group, *Science (Washington, DC, U. S.)*, 2016, **351**, 252-256; aa) R.-Y. Zhu, L.-Y. Liu and J.-Q. Yu, Highly Versatile β -C(sp₃)-H Iodination of Ketones Using a Practical Auxiliary, *J. Am. Chem. Soc.*, 2017, **139**, 12394-12397.

10. S. C. Rajappan, D. R. McCarthy, J. P. Campbell, J. B. Ferrell, M. Sharafi, O. Ambrozaite, J. Li and S. T. Schneebeli, Selective Monofunctionalization Enabled by Reaction-History-Dependent Communication in Catalytic Rotaxanes, *Angew. Chem. Int. Ed.*, 2020, **59**, 16668-16674.

11. a) A. Martinez-Cuevza, D. Bautista, M. Alajarín and J. Berna, Enantioselective Formation of 2-Azetidinones by Ring-Assisted Cyclization of Interlocked N-(alpha-Methyl)benzyl Fumaramides, *Angew. Chem. Int. Ed.*, 2018, **57**, 6563-6567; b) M. Calles, J. Puigcerver, D. A. Alonso, M. Alajarín, A. Martinez-Cuevza and J. Berna, Enhancing the selectivity of prolinamide organocatalysts using the mechanical bond in [2]rotaxanes, *Chem Sci*, 2020, **11**, 3629-3635; c) N. Pairault, H. Zhu, D. Jansen, A. Huber, C. G. Daniliuc, S. Grimme and J. Niemeyer, Heterobifunctional Rotaxanes for Asymmetric Catalysis, *Angew. Chem. Int. Ed.*, 2020, **59**, 5102-5107; d) C. Lopez-Leonardo, A. Saura-Sanmartin, M. Marin-Luna, M. Alajarín, A. Martinez-Cuevza and J. Berna, Ring-to-Thread Chirality Transfer in [2]Rotaxanes for the Synthesis of Enantioenriched Lactams, *Angew. Chem. Int. Ed.*, 2022, **61**, e202209904.

12. S. Amano, S. D. P. Fielden and D. A. Leigh, A catalysis-driven artificial molecular pump, *Nature*, 2021, **594**, 529-534.

13. E. Liu, S. Cherraben, L. Boulo, C. Troufflard, B. Hasenkopf, G. Vives and M. Sollogoub, A molecular information ratchet using a cone-shaped macrocycle, *Chem*, 2023, **9**, 1147-1163.

14. a) N. Basilio, L. García-Río, J. R. Leis, J. C. Mejuto and M. Pérez-Lorenzo, Novel catalytic effects in ester aminolysis in chlorobenzene, *Chem. Commun.*, 2005, DOI: 10.1039/B504629G, 3817-3819; b) N. Basilio, L. García-Río, J. C. Mejuto and M. Pérez-Lorenzo, A New Reaction Pathway in the Ester Aminolysis Catalyzed by Glymes and Crown Ethers, *J. Org. Chem.*, 2006, **71**, 4280-4285; c) R. D. Gandour, D. A. Walker, A. Nayak and G. R. Newkome, Catalysis of ester aminolysis by macrocyclic ionophores, *J. Am. Chem. Soc.*, 1978, **100**, 3608-3609; d) J. C. Hogan and R. D. Gandour, The remarkable catalytic power of glymes in ester aminolysis carried out in nonpolar media, *J. Am. Chem. Soc.*, 1980, **102**, 2865-2866; e) W. P. Jencks and J. Carriuolo, General Base Catalysis of the Aminolysis of Phenyl Acetate, *J. Am. Chem. Soc.*, 1960, **82**, 675-681.

15. a) R. Hertzberg, G. Monreal Santiago and C. Moberg, Synthesis of the β 3-Adrenergic Receptor Agonist Solabegron and Analogous N-(2-Ethylamino)- β -amino Alcohols from O-Acylated Cyanohydrins - Expanding the Scope of Minor Enantiomer Recycling, *J. Org. Chem.*, 2015, **80**, 2937-2941; b) C. Moberg, Minor enantiomer recycling - a strategy to improve enantioselectivity, *Pure Appl. Chem.*, 2016, **88**, 309-316; c) Y.-Q. Wen, R. Hertzberg, I. Gonzalez and C. Moberg, Minor Enantiomer Recycling: Application to Enantioselective Syntheses of Beta Blockers, *Chem. - Eur. J.*, 2014, **20**, 3806-3812; d) E. Wingstrand, A. Laurell, L. Fransson, K. Hult and C. Moberg, Minor Enantiomer Recycling: Metal Catalyst, Organocatalyst and Biocatalyst Working in Concert, *Chem. Eur. J.*, 2009, **15**, 12107; e) C. Moberg, Recycling in Asymmetric Catalysis, *Acc. Chem. Res.*, 2016, **49**, 2736-2745.

16. N. Y. Shin, J. M. Ryss, X. Zhang, S. J. Miller and R. R. Knowles, Light-driven deracemization enabled by excited-state electron transfer, *Science*, 2019, **366**, 364-369.

17. P. Demay-Drouhard, K. Du, K. Samanta, X. Wan, W. Yang, R. Srinivasan, A. C. H. Sue and H. Zuilhof, Functionalization at Will of Rim-Differentiated Pillar[5]arenes, *Org. Lett.*, 2019, **21**, 3976-3980.

18. T. Ogoshi, Synthesis of novel pillar-shaped cavitands "Pillar[5]arenes" and their application for supramolecular materials, *Journal Incl. Phenomen. Macrocyclic Chem.*, 2012, **72**, 247-262.

19. a) P. J. Cragg and K. Sharma, Pillar[5]arenes: fascinating cyclophanes with a bright future, *Chem. Soc. Rev.*, 2012, **41**, 597-607; b) K. Yang, S. Chao, F. Zhang, Y. Pei and Z. Pei, Recent advances in the development of rotaxanes and pseudorotaxanes based on pillar[n]arenes: from construction to application, *Chem. Commun.*, 2019, **55**, 13198-13210.

20. T. Ogoshi, K. Demachi, K. Kitajima and T.-a. Yamagishi, Monofunctionalized pillar[5]arenes: synthesis and supramolecular structure, *Chem. Commun.*, 2011, **47**, 7164-7166.

21. a) S. D. P. Fielden, D. A. Leigh, C. T. McTernan, B. Pérez-Saavedra and I. J. Vitorica-Yrezabal, Spontaneous Assembly of Rotaxanes from a Primary Amine, Crown Ether and Electrophile, *J. Am. Chem. Soc.*, 2018, **140**, 6049-6052; b) M. Sharafi, K. T. McKay, M. Ivancic, D. R. McCarthy, N. Dudkina, K. E. Murphy, S. C. Rajappan, J. P. Campbell, Y. Shen, A. R. Badireddy, J. Li and S. T. Schneebeli, Size-Selective Catalytic Polymer Acylation with a Molecular Tetrahedron, *Chem*, 2020, **6**, 1469-1494.

22. I. Nierengarten, E. Meichsner, M. Holler, P. Pieper, R. Deschenaux, B. Delavaux-Nicot and J.-F. Nierengarten, Preparation of Pillar[5]arene-Based [2]Rotaxanes by a Stopper-Exchange Strategy, *Chem. Eur. J.*, 2018, **24**, 169-177.

23. , Jaguar, version 8.8. *Journal*, 2015.

24. E. R. Johnson, S. Keinan, P. Mori-Sánchez, J. Contreras-García, A. J. Cohen and W. Yang, Revealing noncovalent interactions, *J. Am. Chem. Soc.*, 2010, **132**, 6498-6506.

25. P. Kuzmić, Program DYNAFIT for the Analysis of Enzyme Kinetic Data: Application to HIV Proteinase, *Analytical Biochem.*, 1996, **237**, 260-273.

26. a) A. M. Albrecht-Gary, Z. Saad, C. O. Dietrich-Buchecker and J. P. Sauvage, Interlocked macrocyclic ligands: a kinetic catenane effect in copper(I) complexes, *J. Am. Chem. Soc.*, 1985, **107**, 3205; b) A. H. Parham, B. Windisch and F. Vögtle, Chemical Reactions in the Axle of Rotaxanes – Steric Hindrance by the Wheel, *Europ. J. Org. Chem.*, 1999, **1999**, 1233-1238; c) T. Oku, Y. Furusho and T. Takata, Rotaxane-stabilized thiophosphonium salt from disulfide and phosphine, *Org Lett*, 2003, **5**, 4923-4925; d) E. A. Neal and S. M. Goldup, Chemical consequences of mechanical bonding in catenanes and rotaxanes: isomerism, modification, catalysis and molecular

machines for synthesis, *Chem Commun (Camb)*, 2014, **50**, 5128-5142; e) F. C. Hsueh, C. Y. Tsai, C. C. Lai, Y. H. Liu, S. M. Peng and S. H. Chiu, N-Heterocyclic Carbene Copper(I) Rotaxanes Mediate Sequential Click Ligations with All Reagents Premixed, *Angew. Chem. Int. Ed.*, 2020, **59**, 11278-11282; f) B. Leforestier, M. R. Gyton and A. B. Chaplin, Oxidative Addition of a Mechanically Entrapped C(sp)-C(sp) Bond to a Rhodium(I) Pincer Complex, *Angew. Chem. Int. Ed.*, 2020, **59**, 23500-23504.

27. S. Zhang, W. Li, J. Luan, A. Srivastava, V. Carnevale, M. L. Klein, J. Sun, D. Wang, S. P. Teora, S. J. Rijpkema, J. D. Meeldijk and D. A. Wilson, Adaptive insertion of a hydrophobic anchor into a poly(ethylene glycol) host for programmable surface functionalization, *Nat Chem*, 2023, **15**, 240-247.

[View Article Online](#)
DOI: 10.1039/D3SC04412B

